9. SITE 801[1]

Shipboard Scientific Party[2]

HOLE 801C

Date occupied: 23 June 1992

Date departed: 26 June 1992

Time on hole: 2 days, 6 hr, 43 min

Position: 186.36°38.538′N, 156°21.588′E

Bottom felt (rig floor, m; drill-pipe measurement): 5685.2

Distance between rig floor and sea level (m): 11.2

Water depth (drill-pipe measurement from sea level, m): 5674.2

Total depth (rig floor, m): 6279.50

Penetration (m): 594.30

Comments: Logging and packer experiment

Principal results: The *JOIDES Resolution* arrived at Site 801 on 23 June 1992. Hole 801C, already cored and cased into middle Jurassic oceanic crust on Leg 129, was reentered to conduct downhole measurements of the basement section as these were not accomplished during Leg 129. Reentry was easily accomplished as the cone was visible at the seafloor and the casing appeared to be in good shape. The first logging run with the geophysical string and LDGO temperature tool went to 7 m above total depth (TD) of the hole. Uniformly high velocity and high, but variable, resistivity values were measured throughout. The exception to this was within the hydrothermal zone located halfway down the hole, which separates the upper alkalic basalts from the lower tholeiitic basalts, where both velocity and resistivity were erratic. Temperature data tentatively indicate no significant underpressure and water downflow into the hole. The next Formation MicroScanner (FMS) run also penetrated to 7 m above hole TD, but the following FMS runs and the geochemical run bottomed 40 m above hole TD, as a result of a bridge that developed during the first FMS run. These various high-quality data provide an extraordinary amount of detail on the geochemical and physical characteristics of the alkalic basalts, tholeiitic basalts, and the intervening hydrothermal zone. Results at a previous site indicate that we may be able to recover information about the magnetic polarity of the basalts from the FMS magnetometer data.

With logging operations completed, the permeability test was conducted with the TAM straddle packer settled at three different depths in the hole. We tentatively conclude from the packer experiment that the hydrothermal unit halfway down the hole, and possibly the lower alkali basalt section, are extremely permeable; the tholeiitic basalts below, are relatively impermeable. Our first two packer sets were just below the casing bottom. The pressure records at the rig floor for these sets all indicate an extremely permeable zone somewhere below the packer. However, no downhole pressure data were recorded because of a clock malfunction. Our third set was attempted just below the hydrothermal unit and was not successful because of a ruptured packer element. When we attempted to inflate the packer, the 6200-m-long drill string was lifted several meters uphole instead. This indicated to us that we were pumping through the ruptured packer element into the bottom of an impermeable hole, and the result was to jack up the drill string. When we attempted to inflate the packer again, at the original packer set level just below casing on the way out of the hole, the drill string remained immobile, thus indicating that we were pumping through the ruptured packer element and into the permeable hydrothermal unit, now located below the bottom hole assembly. Several cuts were observed near the bottom of the pacer element when it was retrieved at the rig floor.

BACKGROUND AND OBJECTIVES

Hydrogeology, Structure, and Physical Properties of Oceanic Crust

Several JOIDES panel white papers, two COSOD reports, and the Ocean Drilling Program (ODP) Long-Range Plan agree that a primary goal of ODP should be to characterize the petrology, hydrogeology, structure, and physical properties of typical oceanic crust. The COSOD II report specifically notes the fundamental importance of determining the hydrogeologic properties and the state of stress in the oceanic crust. The LITHP Long Range Planning Document lists the characterization of the in-situ physical properties of Seismic Layer 2 as one of the prime objectives to be accomplished by scientific ocean drilling.

The standard model for the hydrologic evolution of oceanic crust is elegantly simple and qualitatively accounts for many geophysical observations. In this model, newly created oceanic crust is very hot, very porous, and very permeable; consequently, hydrothermal circulation is vigorous. Associated with this hydrothermal flux is mass flux into and out of the formation, resulting in black smokers on the seafloor and alteration of the upper 1 km or more of crust. As the crust ages, seismic velocity and bulk density values increase, porosity and permeability decrease, and magnetic minerals oxidize. Hydrothermal circulation wanes substantially as a result of a decrease in crustal temperature and permeability as well as the accumulation of relatively low-permeability sediment cover.

Hydrothermal convection through the seafloor is not restricted to areas immediately adjacent to spreading centers, but it continues within ridge flanks covered by sediments for tens of millions of years (e.g., Williams et al., 1974; Anderson et al., 1979; Mottl et al., 1983; Becker et al., 1985; Fisher et al., 1990). Although less vigorous than its axial counterpart, off-axis circulation may comprise more than 80% of the total seawater flux through oceanic crust (Morton and Sleep, 1985; Fehn and Cathles, 1986; COSOD II, 1987). It may be responsible for the formation of some manganese crusts (Fehn, 1986), and may determine much of the seismic stratigraphy of the oceanic crust (Carlson and Herrick, 1990).

Our understanding of the hydrogeology of off-axis circulation has been hampered by a dearth of direct measurements of the bulk permeability in the upper oceanic crust. No such direct measurements have ever been made within oceanic crust older than 12 Ma, a total area equal to about 40%–50% of the surface of the planet. Potential variations in crustal permeability have enormous implications for the flux of heat out of the Earth's interior, and for the geochemical and water mass flux through older oceanic crust and the overlying sediments.

To decipher the interactions between hydrogeology, structure, and physical properties in the aging of oceanic crust, a minimum program is to study four typical end-member situations: young

[1] Premoli Silva, I., Haggerty, J., Rack, F., et al., 1993. *Proc. ODP, Init. Repts.*, 144: College Station, TX (Ocean Drilling Program).

[2] Shipboard Scientific Party is as given in the list of participants preceding the contents.

crust created at slow and fast spreading rates, and old crust created at slow and fast spreading rates. The first three of these situations have been accomplished at Holes 395A (young and slow), 504B (young and fast), and 418A (old and slow, although permeability was not determined). The missing end member is old crust formed at a fast spreading rate. Until Leg 129 drilled Hole 801C, such holes either had large uncertainties in their basement ages (Holes 595A and 765D) or sampled crust created just after continental rifting (Holes 534A and 765D), and thus were unsuitable as typical of normal oceanic crust.

Site 801

Hole 801C sampled a Middle Jurassic open-ocean spreading system now located in the northwestern Pacific Ocean (Fig. 1). Its biostratigraphic and radiometric ages match closely to the age predicted by extrapolating magnetic anomaly isochrons. It is the oldest oceanic crust (158–165 Ma) sampled to date, and it was formed at a whole spreading rate between 15 and 20 cm/yr. Although basement penetration in Hole 801C is less than at the other end-member sites, downhole measurements here would help to complete the characterization of oceanic crustal end members.

A summary stratigraphic diagram of Site 801 is shown in Figure 2. All but the uppermost 56 m of the section consists of Cretaceous and Jurassic sediments and Jurassic volcanic basement (Shipboard Scientific Party, 1990). Beneath a thick section of mid-Cretaceous (Albian) volcaniclastics lies a nearly uninterrupted section of Valanginian to Bathonian (130–165 Ma) deep-sea pelagic sediments. The basal Bathonian sediments are interbedded with extrusive basalts at the top of the igneous section recovered in Hole 801B.

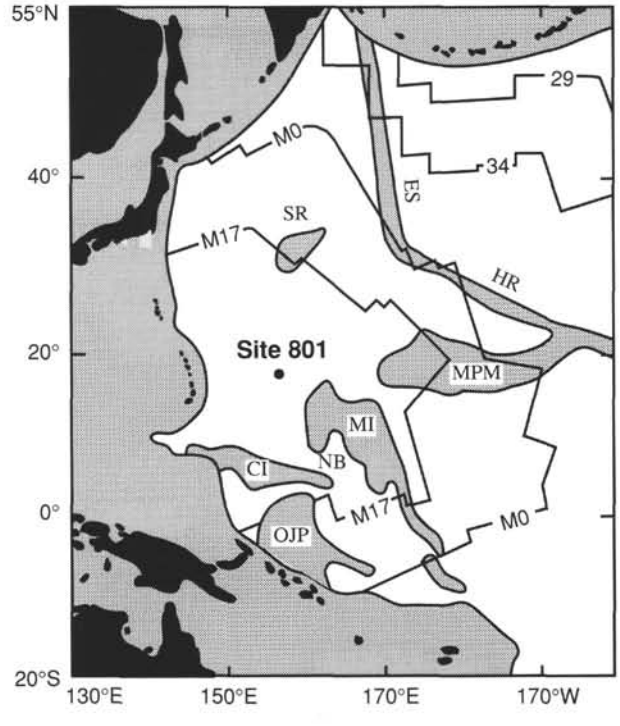

Figure 1. Location of Site 801. White areas represent normal Pacific oceanic crust formed at spreading centers in the Mesozoic. Bedrock isochrons are determined from magnetic anomaly lineation mapping on the Pacific Plate (Larson et al., 1985) and are superimposed on groups of islands, atolls, and guyots in the northwestern Pacific Ocean. Shaded areas represent volcanic edifices with thickened crustal sections as well as younger areas north and west of the Pacific Plate subduction zones. Feature abbreviations are as follows: Caroline Islands (CI), Ontong Java Plateau (OJP), Marshall Islands (MI), Nauru Basin (NB), Mid-Pacific Mountains (MPM), Shatsky Rise (SR), Hawai-

Holes 801B and 801C penetrated a combined total of 131 m of Jurassic basement, 113 m of which are exposed for downhole measurements beneath the bottom of casing in Hole 801C. Basement recovery from Hole 801C was about 60%, and 33 cooling units were recognized from the recovered samples. The uppermost basalts exposed in Hole 801C have alkalic affinities and are 4–14 m.y. younger than the underlying tholeiites. The alkalic and tholeiitic sequences are separated by a fossilized hydrothermal deposit, enriched in silicon and iron, that formed on the Middle Jurassic seafloor after extrusion of the tholeiites and before the alkalic basalts. Some of the tholeiites directly below the hydrothermal deposit are highly fractured and extremely altered, and they exhibit a late, oxidative type of alteration, suggestive of proximity to a hydrothermal system.

Questions To Be Answered by Downhole Measurements at Hole 801C

Questions in hydrogeology are the following: What is the permeability of old oceanic crust? What was the original porosity structure? Do convection and formation underpressure exist here? Answers to the first and third questions are usually assumed to be zero and no. Any indications to the contrary will have major implications for global heat flux, water mass flux, and associated geochemical flux in old oceanic crust.

Tectonics and magnetic reversal stratigraphy questions are the following: What is the direction of in-situ stress in the old Pacific Plate, if any such finite stress exists? Is the Jurassic Magnetic Quiet Zone caused by many reversals, or none?

Seismology questions are the following: What is the detailed seismic velocity structure of the uppermost portion of old oceanic crust? How is this related to density and electrical resistivity of the same crustal section? How are all of these geophysical parameters related to volcanic flow morphology and basalt alteration? Do hole conditions, casing conditions, and reentry cone visibility make this a viable site for deployment of a "permanent" downhole seismometer? This location fills a major blind spot in the worldwide seismic arrays used to study lower mantle and core/mantle boundary structure by recording deep mantle ray paths of teleseismic earthquakes.

Last of all, from a geochemical point of view, what is the final, integrated chemical composition of oceanic crust?

OPERATIONS

Site 877 to Site 801

JOIDES Resolution departed Site 877, on Wodejebato Guyot, at 1030L (L = local time) on 21 June 1992. The average transit speed of 11.7 kt over the 636-nmi voyage yielded an arrival at Site 801 at 1500L on 23 June 1992. Speed was reduced and the ship was maneuvered to the geographic coordinates of the reentry cone of Hole 801C by GPS navigation. At 1545L the vessel was stopped and the thrusters and hydrophones were lowered. Once in dynamic positioning (DP) mode, the ship was positioned more precisely and a positioning beacon was launched at 1630L on 23 June 1992.

Hole 801C

A 3-day program of downhole measurements was scheduled at Hole 801C as an alternate site for Leg 144, if time was available; this hole was drilled on Leg 129. The drilling objectives for Site 801 were reached, but operating time on Leg 129 ran out before the planned downhole-measurements program of logging and permeability experiments could be accomplished. Good hole

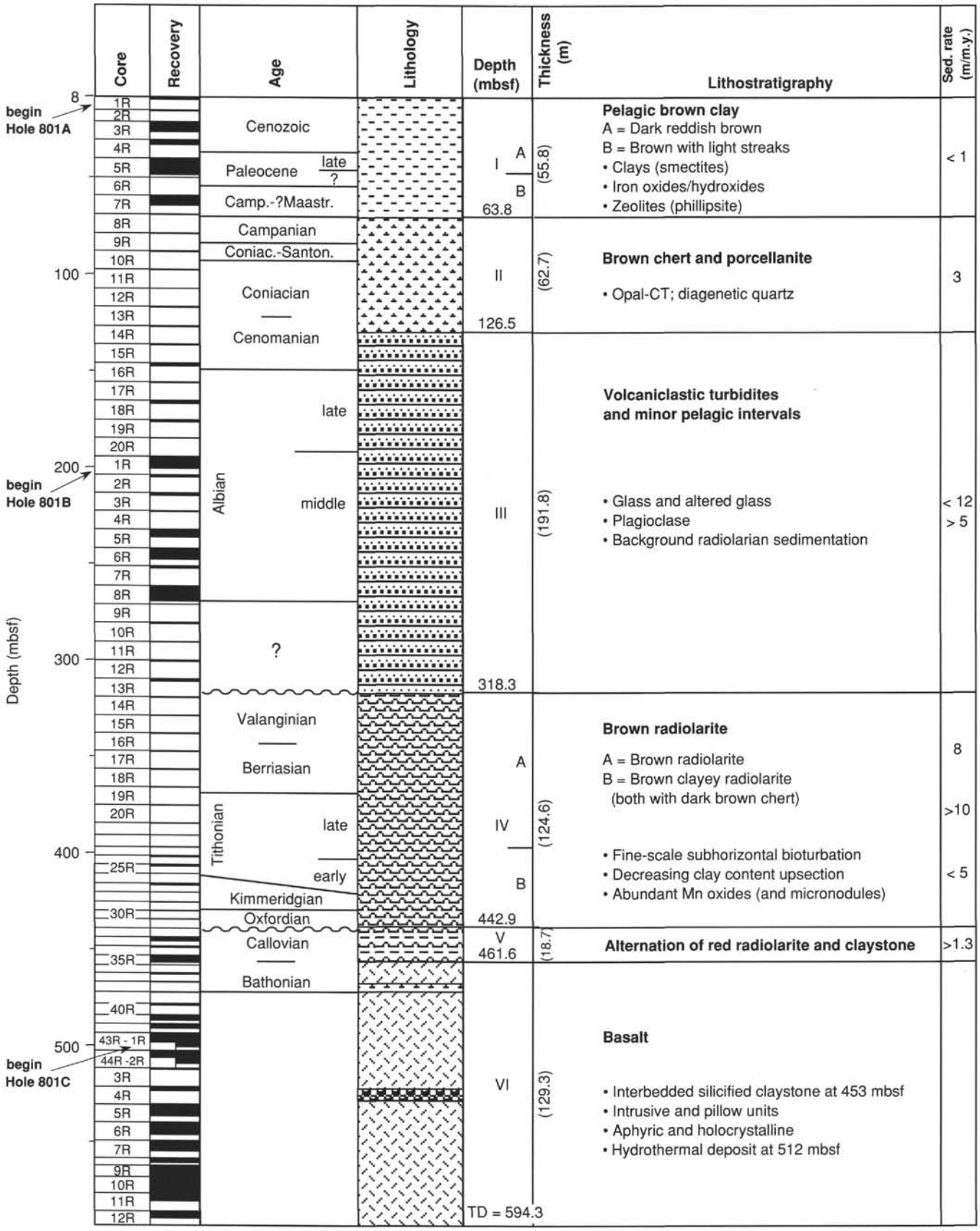

Figure 2. Coring record, biostratigraphic ages, lithostratigraphy, and sedimentation rates of Site 801 compiled from Holes 801A, 801B, and 801C. TD = total depth.

conditions were anticipated for this reentry on Leg 144 because the hole was cased into basaltic basement rocks.

An open-ended bottom hole assembly (BHA) with a reentry/clean-out bit was used because no drilling or hole cleaning was anticipated. The pipe trip was long because of the deep water depth (5685 m) and because much of the pipe had not been measured at the shallower sites earlier in the leg. In addition, 24 joints of new 5-in. pipe were removed from the hold to lengthen the working string to the depth of the planned packer experiments. Before reentry depth had been reached, a breakdown of the 5½-in. piperacker delayed the trip by an additional 30 min. The pipe trip was also interrupted to deploy the vibration-isolated television (VIT), so that the BHA and VIT would reach reentry depth at about the same time.

The reentry cone target was located by VIT sonar almost immediately, and the relative positions confirmed that the positioning beacon had landed only about 45 m from the cone. About 1.25 hr of maneuvering was required to close the distance and swing the pipe over the cone for reentry. During that time, the circulating head was rigged and the combination of a plastic "pig" and a rubber cementing top plug was pumped through the drill string to dislodge any loose rust scale. Reentry into Hole 801C was made at 0715L on 24 June 1992.

While the VIT was recovered to the ship, four stands of pipe were run to put the BHA entirely below the seafloor level. The logging sheaves then were rigged and logging operations began. The geophysical tool string found its way to within about 7 m of the total depth of Hole 801C. Temperatures in the undisturbed water column were logged with the LDGO self-contained temperature recorder as the tool descended. Good logs of all geophysical parameters were recorded from set-down to the casing shoe, an open-hole interval of about 108 m. The second run with the Formation MicroScanner (FMS) tool reached about the same total depth as the first pass. Abnormal readings on the caliper logs indicated that the arms may have been fouled during the lower part of the first FMS run. As multiple runs were desired for more complete coverage of the borehole wall, the pads were retracted and the tool was lowered again after reaching the casing. The tool appeared to operate normally, but it would not pass a newly formed bridge in the hole about 65 m below the casing shoe. The second and third FMS runs were made from that depth, and excellent quality data were recorded. The FMS tool was tripped to the surface and exchanged for the geochemical tool string. That tool also was stopped at the bridge, which apparently formed before the second run of the FMS tool. The geochemical log was recorded up into casing and can be tied in with the interval logged on Leg 129 in Hole 801B.

With logging operations completed, the sheaves were rigged down and preparations were made for the scheduled permeability tests. About 4 hr were spent in pressure-testing the rig's surface equipment and in stopping minor leaks. Another set of pigs was pumped through the drill string because of the newly added, used drill pipe. The packer then was lowered into the open hole for the first set. The caliper logs indicated a relatively smooth area, nearly the same diameter as the bit at about 22 m below the casing shoe (501 m below seafloor [mbsf]) in the open hole.

The TAM straddle packer (TSP) go-devil, with a Kuster downhole pressure recorder, was pumped into place to actuate inflation of the packer. Pressure was held for a short time to establish a hydrostatic base-line pressure on the record and to test the pressure integrity of the entire system. The drill string then was pressured up to inflate the packer, with all indications of a normal set. Two pulse tests were attempted after the initial set; pressure bleed-off was very rapid, indicating high permeability. Two constant-rate injection tests followed, with pressure buildup and decay rates indicating good tests and high permeability. To help ensure that the hydraulic seal of the packer would not be doubted, the packer then was unseated and moved up the hole about 2 m to 494 mbsf. It was reset with the same indications of normal setting (holding 15,000 to 20,000 lb weight). Three pulse tests were accomplished with the same rapid decay as on the first set.

A trip was then made with the coring line to retrieve the go-devil and pressure recorder. Unfortunately, the record of the Kuster gauge (the only one aboard rated to 15,000 psi) was useless because of a suspected malfunction of the clock; however, usable data were recorded by surface instrumentation. A second go-devil was dressed with a different clock on the same pressure gauge and also with the clock from the first run on a 12,000 psi-pressure gauge that would be operating near its maximum limit. While the go-devil was being prepared, the packer was lowered to the depth of the second planned test, about 63 m below the shoe (542 mbsf).

After the go-devil was pumped into place at the TSP, inflation was attempted again. This time the system held about 200 psi for several minutes after the go-devil landed, but normal indications of inflation did not appear when more fluid was pumped to raise the pressure in the drill string. Inflation pressures were held only briefly before the drill-string weight indicator dropped. This was interpreted to indicate that the packer element was acting as a sliding piston and "jacking" the pipe up the hole. When the element is torn or punctured, it will partially inflate while transmitting fluid into the open hole below it through the rupture. After several attempts to set the packer, it was raised to the position where it had been successfully set earlier to verify that the present difficulty was not in the setting location. Again the packer failed to inflate, but a constant circulating rate was maintained without pushing the pipe uphole because of the high permeability of the hole immediately below the packer.

After confirmation that the element was "blown," the coring line was run to retrieve the go-devil. The go-devil was found to be stuck and no amount of pulling and/or jarring could dislodge it. The safety shear pin of the pulling tool was sheared, and the coring line was recovered as the crew prepared for a "wet trip."

Surprisingly, the drill pipe came dry, indicating that the rupture in the packer element was sufficient to drain the water from the drill string faster than the pipe was pulled. The interior of the deep-water portion of the drill string was coated with anti-corrosion chemical as it was tripped. When the TSP cleared the rig floor, the go-devil was in its proper setting position, extending beyond the reentry/clean-out bit, and still firmly stuck. The weight of the lower stand of drill collars had to be used to force the seals out of their seats. The packer element showed four or five deep vertical cuts in the outer covering over most of its length with one or two possible punctures at the ends of gashes. Though water continued to leak from one of those holes in the outer covering during disassembly, the breach in the inner bladder could not be located visually. Inspection of the go-devil revealed the seals and landing ring to be in good condition. The presence of rust grit at the seals was blamed for sticking, although only a small amount was found.

The beacon had been recalled during the pipe trip. When the rig floor were secured and the thrusters and hydrophones raised, the vessel departed for the next site. Official departure was at 1315L on 26 June 1992.

DOWNHOLE MEASUREMENTS

Log Types, Processing, Reliability, and Resolution

Logs were obtained in Hole 801C, which was drilled into Middle Jurassic oceanic crust in the Pigafetta Basin during Leg 129 (Fig. 3). These logs consisted of one pass with the geophysical tool string, which included the Lamont-Doherty temperature tool at its base, three passes with the Formation MicroScanner

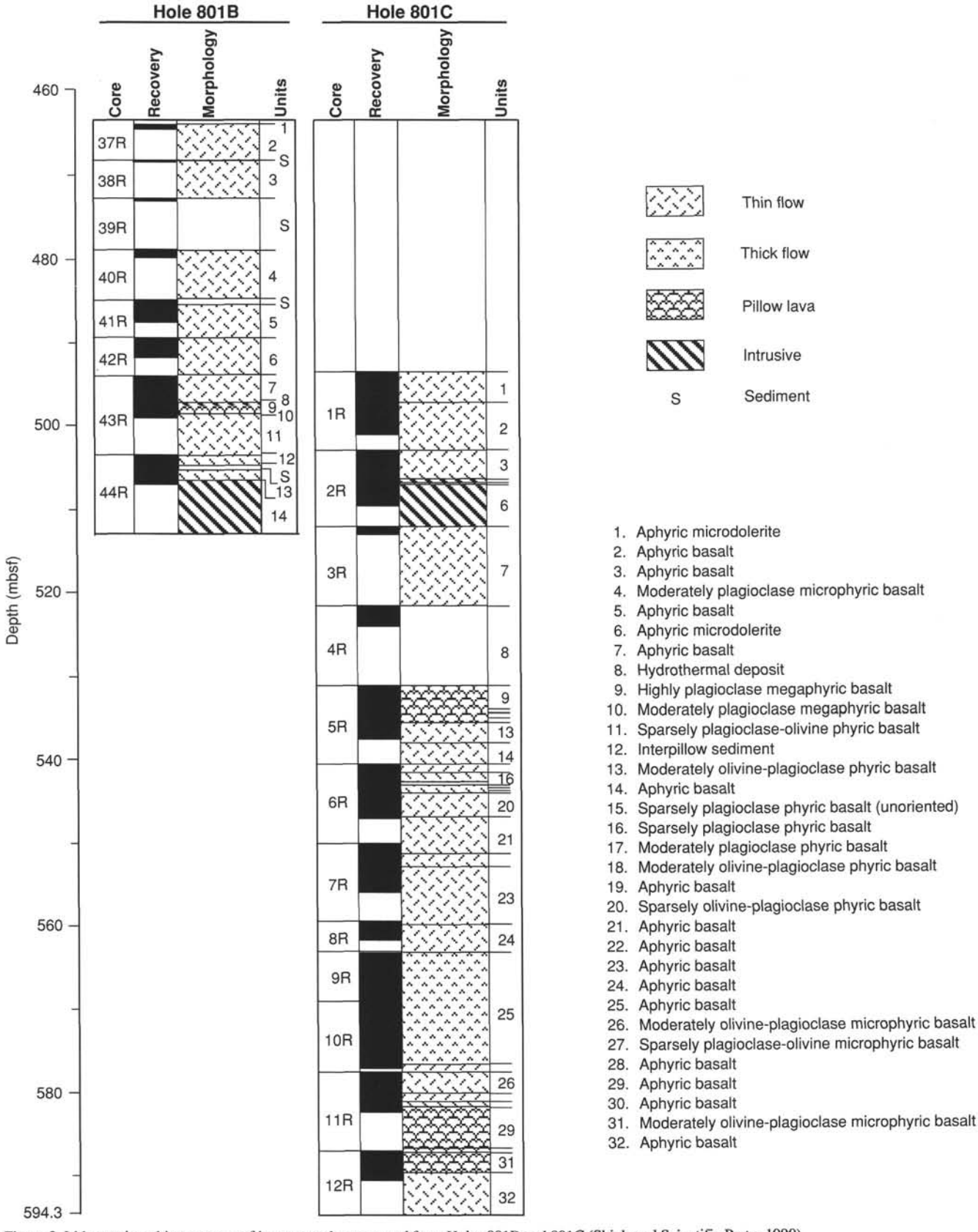

1. Aphyric microdolerite
2. Aphyric basalt
3. Aphyric basalt
4. Moderately plagioclase microphyric basalt
5. Aphyric basalt
6. Aphyric microdolerite
7. Aphyric basalt
8. Hydrothermal deposit
9. Highly plagioclase megaphyric basalt
10. Moderately plagioclase megaphyric basalt
11. Sparsely plagioclase-olivine phyric basalt
12. Interpillow sediment
13. Moderately olivine-plagioclase phyric basalt
14. Aphyric basalt
15. Sparsely plagioclase phyric basalt (unoriented)
16. Sparsely plagioclase phyric basalt
17. Moderately plagioclase phyric basalt
18. Moderately olivine-plagioclase phyric basalt
19. Aphyric basalt
20. Sparsely olivine-plagioclase phyric basalt
21. Aphyric basalt
22. Aphyric basalt
23. Aphyric basalt
24. Aphyric basalt
25. Aphyric basalt
26. Moderately olivine-plagioclase microphyric basalt
27. Sparsely plagioclase-olivine microphyric basalt
28. Aphyric basalt
29. Aphyric basalt
30. Aphyric basalt
31. Moderately olivine-plagioclase microphyric basalt
32. Aphyric basalt

Figure 3. Lithostratigraphic summary of igneous rocks recovered from Holes 801B and 801C (Shipboard Scientific Party, 1990).

(FMS), and one pass with the geochemical tool string. The geophysical tool string and the first pass with the FMS extended to within about 7 m of the bottom of the hole at 594 mbsf (6279 m below rig floor [mbrf]). Apparently, during the first FMS pass, contact pads dislodged rocks that formed a bridge located about 40 m above the bottom of the hole, which the subsequent logging runs could not pass. The differing locations of each of the tools on each of the tool strings means that the lower boundary of logging data from each tool is different (see diagram of tool strings in "Explanatory Notes" chapter, this volume). All logging runs extended up to the base of the Leg 129 casing string at 481 mbsf (6166 mbrf). In addition, the geochemical run extended up within the casing to 281 mbsf, thus sampling the geochemical characteristics of the entire Lower Cretaceous and Jurassic sedimentary section and providing an opportunity for correlating this log with the geochemical log run during Leg 129 about 20 m away in Hole 801B. Because of the extensive post-cruise processing necessary for interpreting these logs within drill pipe, they are not displayed or discussed in this volume.

The logs were located relative to each other and to the bottom of the Leg 129 casing string. This first required determination of the exact depth of the bottom of casing, which was uncertain because a 3-m-long slip joint in the casing string may not have opened during casing emplacement or subsequently. Leg 129 drilled a 14¾-in. diameter hole to accept the casing to a total depth of 491 mbsf (6176 mbrf), and then began coring operations below that point with a 9⅞-in. diameter bit. The base of the wider casing hole was located on the precise caliper log of the FMS string, and also on the caliper log of the geophysical string (Fig. 4). The bottom of casing was located 10 m higher, at 481 mbsf (6166 mbrf), where the caliper of the FMS tool string entered the casing. The casing bottom also was located with an open caliper during the geophysical run and with the iron log during the geochemical run. This is the same depth estimated for the casing bottom by the Leg 129 scientists.

These data could then be used to correlate the logs together. This intercorrelation was confirmed with intercomparisons among the natural gamma-ray logs on each tool string and with the distinctive base of the hydrothermal unit in the caliper data from both the geophysical and FMS strings. This intercorrelation and calibration to the depth of casing required 7 m to be subtracted from the geophysical string logging depths, and 9 m from the geochemical and FMS string logging depths. A seafloor depth below the 5685-m rig floor was also subtracted from the logging depths to obtain a depth below seafloor.

Generally, the data from all of these logging runs are of high quality, with the exception of the FMS and caliper data during the first FMS run. Apparently, the caliper arms did not open completely during this run; therefore, the resistivity signal in the FMS data appears "weak," and the caliper data do not correlate with the subsequent runs.

Sonic Velocity Calculations

The sonic velocity profile as a function of depth in the hole (Fig. 4) was calculated from the traveltime data of four different receivers in the following manner. The traveltimes from the two receivers located at different distances from the sound source were subtracted at each measurement point to obtain the time difference, or delay time, between the two receivers. This was done for both pairs of receivers. The distance between each pair of receivers was then divided by that delay time to obtain the compressional wave velocity between those two receivers. Any velocities below 1500 m/s and above 8000 m/s were discarded. The remaining pairs of velocities then were averaged to obtain the average compressional wave velocity at that point in the formation.

Upon inspection, the four original traveltime plots appeared to be well correlated, and these data did not contain a large number of obviously incorrect traveltime estimates. The resulting velocity profile has reasonable velocities for old oceanic crust of between 5.5 and 6.5 km/s, except for the anomalous decrease in velocity to below 3.0 km/s within the hydrothermal zone. In addition, the overall velocity profile is similar in shape to the bulk density profile and to the inverse of the porosity profile. Thus, this profile is considered to be a good estimate of the compressional wave velocity variation in the basement section of Hole 801C.

Core-log Integration

The basement section in Hole 801C will be described in three units from top to bottom: the alkalic basalts, the hydrothermal zone, and the tholeiitic basalts. The entire section is of Middle Jurassic age, but this almost certainly represents a distinct age progression. The upper alkalic basalts have been dated at 157 ± 0.5 Ma and the lower tholeiitic basalts at 165 ± 4.5 Ma (Pringle, 1992). Thus, the tholeiitic basalts were probably erupted first at a Middle Jurassic spreading center, and the alkalic basalts capped the ridge crest sequence about 5–10 m.y. later with a slightly off-ridge eruption. The hydrothermal zone is undated, but it is probably of some age intermediate between the two different lava sequences.

The Alkalic Basalts

Alkalic basalts were recovered in Hole 801B in Cores 129-801B-37R to -44R, from 463 to 513 mbsf, and about 20 m away in Hole 801C in Cores 129-801C-1R to -3R, from 493 to 522 mbsf (Shipboard Scientific Party, 1990, fig. 3). The casing string was drilled and cemented into the upper part of the alkalic basalts in Hole 801C, so that only the section below 481 mbsf was exposed for open-hole logging. The entire sequence was logged below that level with all the logging runs; the geochemical run extended up into the casing, well above the top of the alkalic basalt sequence. It appears that the underlying hydrothermal zone is about twice as thick as previously described (Shipboard Scientific Party, 1990), extending up to 510 mbsf, although this extended logging definition of the hydrothermal zone actually includes the lowest alkalic basalts recovered in Core 129-801C-3R. This logging evidence will be presented in the next section so that the upper and lower boundaries of the hydrothermal zone can be described together.

The geophysical logs are relatively uniform across the alkalic basalt section from 481 to 510 mbsf, with the exception of a thin unit at about 500 to 502 mbsf. Excluding that thin unit, bulk densities are constant at 2.7 g/cm^3, and compressional wave velocities are relatively constant at 4.8–5.1 km/s (Fig. 4). Both of these values are significantly lower than those found in the underlying tholeiites, but they closely resemble the values measured in the recovered samples of the alkalic basalts (Shipboard Scientific Party, 1990). Porosity is relatively high, with a decreasing downward trend, whereas the shallow resistivity tool measured relatively low values of about 20 Ωm. Resistivity increases dramatically in the underlying tholeiites. Several veins and fractures are apparent in the FMS data. These can probably be correlated with similar features in the core photos of these thick basalt units.

In the stable-element logs, iron is significantly lower than in the tholeiites and calcium is slightly lower (Fig. 5). Both aluminum and silicon have strongly increasing downward trends from 481 to 500 mbsf for unexplained reasons. This is especially puzzling in the aluminum log because of the nonmobile nature of this element. The natural gamma-ray log is unremarkable, except for peaks at 495 and 500 mbsf, with the latter being the largest and probably associated with the thin, anomalous unit mentioned

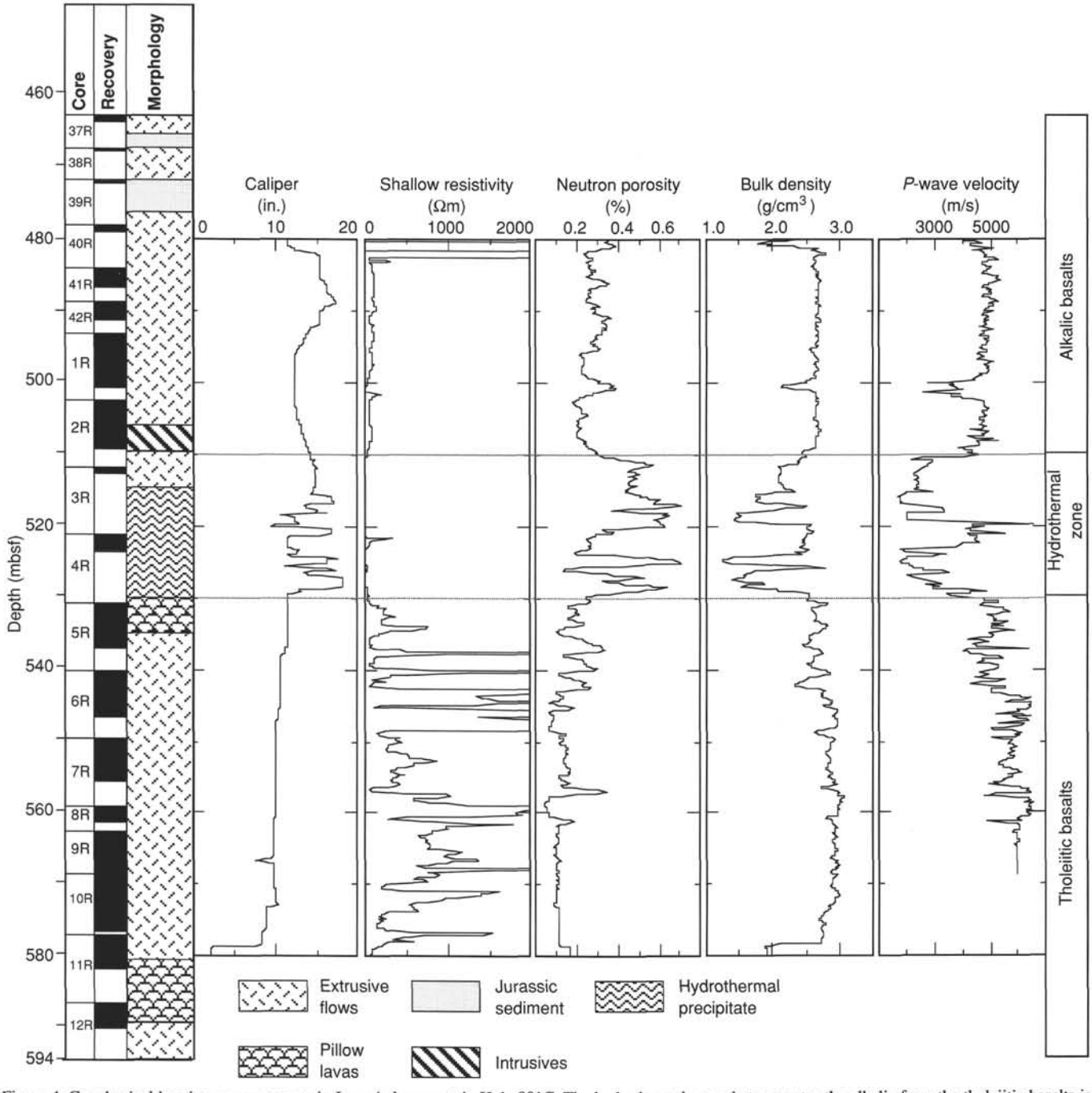

Figure 4. Geophysical logging measurements in Jurassic basement in Hole 801C. The hydrothermal zone that separates the alkalic from the tholeiitic basalts is outlined most prominently in the porosity, density, and compressional (*P*-wave) velocity logs, although the lower boundary is distinct in the caliper log. Shallow-penetration resistivity that shows large increases in the tholeiitic basalts is illustrated. The rock morphology shown here (and in the two succeeding figures) has been reinterpreted on the basis of core-log integration from that determined by core recovery alone during Leg 129.

above (Fig. 6). Most of the natural gamma-ray signal appears to be concentrated in potassium in this section.

The thin unit at 500 to 502 mbsf appears in most of the logs mentioned above as an anomaly, with the exceptions of iron and silicon. This also is not apparent on either of the caliper logs. In the geophysical logs, the thin unit appears as a low in density, velocity, and resistivity, and as a high in porosity. The unit also appears as a low in resistivity in the FMS log. In the chemical logs, this thin unit appears as a low in aluminum and calcium, and as a high in potassium. With the exceptions of the high in potassium and its unremarkable caliper log, the thin unit has a signature identical to the underlying, and much thicker, hydrothermal unit that separates the alkalic and tholeiitic basalt sequences. No evidence of such material, or any other anomalous material is seen in Core 129-801C-1R, which consists of a 7.5-m aphyric microdolerite, grading downward into an aphyric basalt. Thus, the anomalous unit has a maximum thickness of 2 m. However, the relatively consistent pattern among the logs leads us to suggest

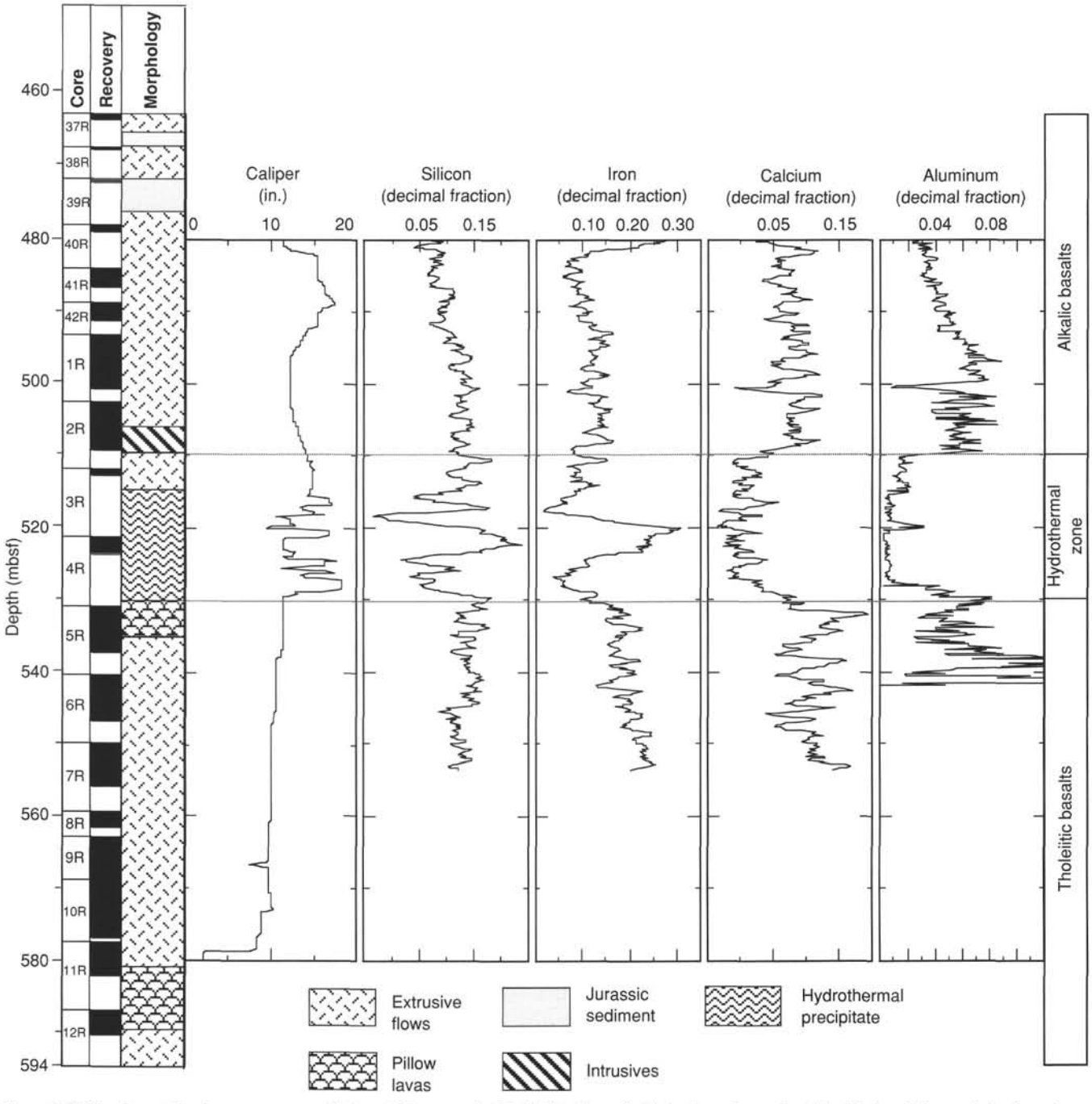

Figure 5. Stable-element logging measurements in Jurassic basement in Hole 801C. The entire hydrothermal zone is outlined in the calcium and aluminum logs, whereas the concentrated, central peaks within that interval in silicon and iron probably correspond to the material recovered in Core 129-801C-4R.

that some fraction of the interval between 500 and 502 mbsf is another very thin hydrothermal unit similar to the one that is described below.

The Hydrothermal Zone

The hydrothermal zone appears to be about 20 m thick; it extends from 510 to 530 mbsf. This zone is delineated in the geophysical logs by anomalous lows in bulk density, *P*-wave velocity, and electrical resistivity and by a high in porosity within this interval. Anomalies of the opposite polarity are situated in the midst of this zone from 520 to 525 mbsf (Fig. 4).

The FMS shows high resistivity from 511 to 513 mbsf, a "banded" appearance from 513 to 516 mbsf, and patchy, high resistivity from 516 to 518 mbsf. The interval from 519 to 529 mbsf is blurred owing to poor contact of the pads with the borehole wall. Both calipers, but especially those of the FMS, exhibit wide variations in hole diameter from 514 to 530 mbsf. The upper boundary of this interval is gradational up to 510 mbsf, whereas the lower boundary is abrupt at 530 mbsf (Fig. 4).

The hydrothermal zone from 510 to 530 mbsf is bounded by sharp, positive anomalies in gamma-ray spectra (potassium) at the top and the bottom (Fig. 6). The zone is marked by uniform lows

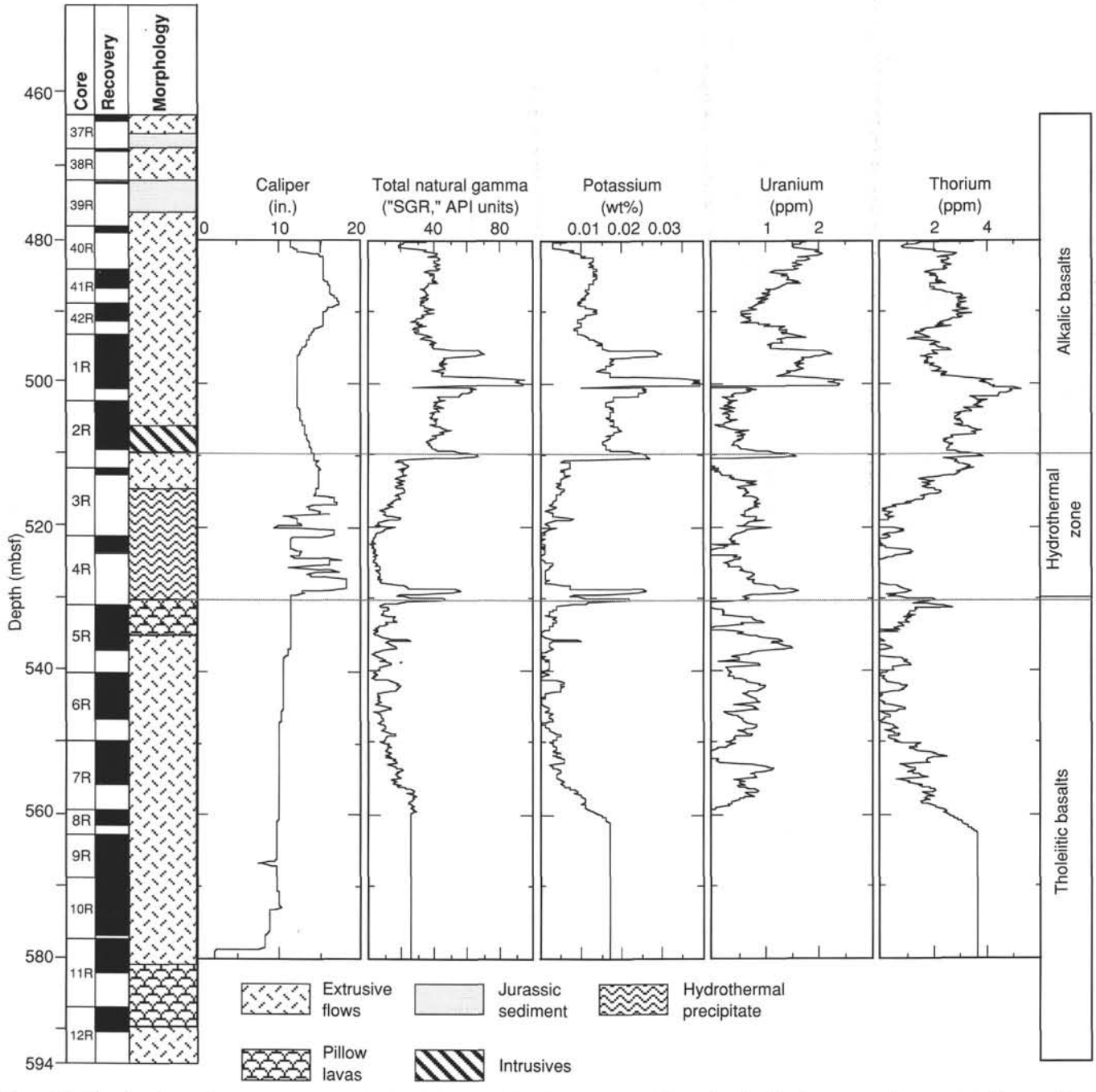

Figure 6. Radioactive-element logging measurements in Jurassic basement in Hole 801C. Most of the radioactive fraction seems to be concentrated in potassium. The hydrothermal zone is bounded by large peaks in total gamma rays and potassium.

in calcium and aluminum across the entire interval. Silicon and iron show large positive anomalies from 520 to 525 mbsf, both flanked above and below by anomalous lows (Fig. 5).

Core recovery within the hydrothermal zone was only 20%, consisting of 1 m of highly altered, aphyric basalt in Core 129-801C-3R (513–522 mbsf), and 3 m of iron oxyhydroxide precipitate in Core 129-801C-4R (522–531 mbsf). In addition, some microdolerite from Core 129-801C-2R may extend down into this interval, but this is not required and is considered unlikely.

We have integrated these cores and logs with the following interpretation. The 3 m of iron oxyhydroxide was recovered from the very top of the interval cored by Core 129-801C-4R (522–525 mbsf), and thus sampled the "internal anomaly" between 520 and 525 mbsf within the hydrothermal zone. The highly altered, aphyric basalt was recovered from near the top of the interval cored by Core 129-801C-3R, probably 513–514 mbsf. Initially, one might question such an interpretation, which requires a basalt interval to have a lower velocity and a higher porosity than a hydrothermal precipitate, or which assumes that the Leg 129 coring depths and the Leg 144 logging depths have been miscorrelated. However, the physical properties of the recovered samples support the above interpretation (Shipboard Scientific Party,

1990). In particular, the compressional wave velocity of the iron oxyhydroxide was measured as 5.1 km/s, whereas that of the overlying, highly altered, aphyric basalt is 3.7 km/s, down from a broad average of 4.6 km/s in the upper alkalic basalts. Measured porosity in the iron oxyhydroxide is a minimum relative to the alkalic basalts, with the exception of one sample, whereas the aphyric basalt within the hydrothermal zone has the maximum measured porosity of any of the alkalic basalts. In addition, thermal conductivity, which is usually inversely proportional to porosity, is two and a half times higher in the iron oxyhydroxide than in any of the basalts recovered anywhere within Hole 801C. The caliper log at 513–514 mbsf is in the "transition" region between the upper alkalic basalts and the main part of the hydrothermal zone. The only anomaly unexplained by this interpretation is the uniform low in aluminum across the entire interval from 510 to 530 mbsf, because aluminum within basalts is a very nonmobile element. Shore-based studies of the chemistry of this basalt (Floyd and Castillo, 1992) and the corrected chemical log to be produced onshore after Leg 144 will be used to validate or deny these interpretations.

If the above interpretations are correct, the following scenario might be envisioned. The hydrothermal precipitate and at least the oldest alkalic basalts are time synchronous, having been erupted up through the 5- to 10-m.y.-old tholeiitic basalts in a slightly off-ridge situation. The hydrothermal system that produced the 20-m-thick chemical precipitate also severely altered the lowest alkalic basalts, essentially incorporating those basalts into the hydrothermal zone. Those alkalic basalts covered the chemical precipitate soon after, or indeed during its formation, and thus preserved it from dissolution. In the intervening 150 m.y., the original chemistry of this 20-m-thick precipitate has migrated, concentrating most of the original iron and silicon into a 5-m-thick "concretion," 3 m of which was recovered in Core 129-801C-4R.

The Tholeiitic Basalts

The tholeiitic basalts extend from 530 mbsf to the bottom of Hole 801C at 594 mbsf. Logging intervals using various tools generally extend upward from somewhere between 555 and 580 mbsf, depending on the location of the tool in the logging string and on the greatest depth of penetration of the particular logging run. As exceptions, the aluminum tool data begin at 540 mbsf, whereas the magnetometer data discussed in another section extend down to 587 mbsf.

Compressional wave velocities and bulk densities increase gradually downward from 530 to 550 mbsf and then remain relatively constant to the bottom of each logging interval. Velocities increase from about 5.0 to 5.8 km/s, whereas densities increase from about 2.6 to 2.8 g/cm^3. Electrical resistivity values increase dramatically (by up to a factor of 10) down to 580 mbsf at the bottom of the logging interval. Porosities decrease gradually downward from 530 to 550 mbsf, and like velocity and density, then remain constant to the bottom of the logging interval at 580 mbsf (Fig. 4).

The gamma-ray (potassium) log is unremarkable, except for a sharp, positive anomaly at the base of the hydrothermal zone that presumably marks the boundary between the iron oxyhydroxide precipitate and the underlying tholeiites (Fig. 6). Aluminum, silicon, and calcium values are all relatively constant in the stable-element logs (Fig. 5). Iron increases downward throughout the logged interval from 530 to 555 mbsf and has generally larger concentrations than in any of the alkalic basalt section. This is significant in several different ways. First, it may indicate that the uppermost tholeiites were the source of much of the iron in the overlying iron oxyhydroxide precipitate. Second, the magnetometer record (discussed elsewhere in detail) shows little influence from the natural remanent magnetization (NRM) of the basalts within the borehole down to 550 mbsf, but large anomalies are present below that level. This is confirmed by the NRM intensities of the recovered basalt samples, which exhibit a sharp increase below 555 mbsf (Wallick and Steiner, 1992).

Downhole Magnetometer Measurements

A three-axis fluxgate magnetometer was attached to the FMS tool. Data about the orientation and strength of the magnetic field within the borehole were collected at 15-cm (0.50 ft) intervals, whereas the FMS image data were obtained at 2.5-mm sampling rate.

The three-component magnetic data (FX is the horizontal "x" component, parallel to the FMS Pad 1 direction; FY is the horizontal "y" component, perpendicular to the Pad 1 direction; and FZ is the vertical "z" component) enable one to calculate horizontal and vertical intensity, inclination, and relative declination (Fig. 7). Generally, the magnetic direction is used to orient the FMS traces with respect to magnetic north, and the NRM of the formation is assumed to be negligible. Within a borehole through rocks having a strong NRM different in direction from the present-day magnetic field, this magnetic orientation is distorted; instead, we acquire valuable information on the NRM directions and intensities of those rocks.

Three runs were conducted with the FMS/magnetometer string after the geophysical logging. Logging Run 1 was from 587 mbsf, nearly the bottom of the hole, up to the bottom of the Leg 129 casing (481 mbsf). The tool did not go below 557 mbsf for Runs 2 and 3, apparently because of a bridge that developed during the first FMS logging run.

Judging from the comparison of the caliper data from FMS Run 1 with those from Runs 2 and 3, and from the geophysical logging, the caliper arms did not open completely during Run 1. However, the fine-scale variations in the observed magnetic field with depth above 557 mbsf were duplicated during the two following FMS/magnetometer passes, indicating that the incomplete arm contact did not affect the magnetometer data.

Above about 495 mbsf, a large amount of disturbance is seen in the downhole magnetic field that was caused by the casing pipe, which was set at 481 mbsf during Leg 129. The magnetometer appears to be recording only the ambient, present-day field between 495 and 550 mbsf, because the horizontal and vertical intensity curves are both very smooth and contain only small anomalies. At about 550 mbsf, sharp decreases in both the vertical and horizontal components of the downhole magnetic field are seen. The amplitude ratio of the horizontal component to the vertical component at this sharp peak is about 1:2, although it is about 1:1 below that level. At about 580 mbsf, sharp increases were seen in both the vertical and horizontal components of the downhole magnetic field.

These features are consistent with the results from the recovered core samples (Shipboard Scientific Party, 1990; Wallick and Steiner, 1992). The NRM intensities measured for the recovered core samples above Section 129-801C-7R-2 (550 mbsf) have low values, whereas those in the cores beginning with Section 129-801C-7R-3, and continuing down to Section 129-801C-12R-3, are generally high (Shipboard Scientific Party, 1990; Wallick and Steiner, 1992). Vertical and horizontal intensity components of a total field anomaly caused by a simple, flat layer would have opposite signs were the layer magnetized at its present-day location (Gallet and Courtillot, 1989). The sharp, well-correlated decreases in both the vertical and horizontal intensity components from 550 to 580 mbsf are caused by strong magnetization of aphyric basalts with reverse-polarity magnetization acquired in the Southern Hemisphere and transported to the Northern Hemisphere by plate motion (Larson and Sager, 1992; Steiner and

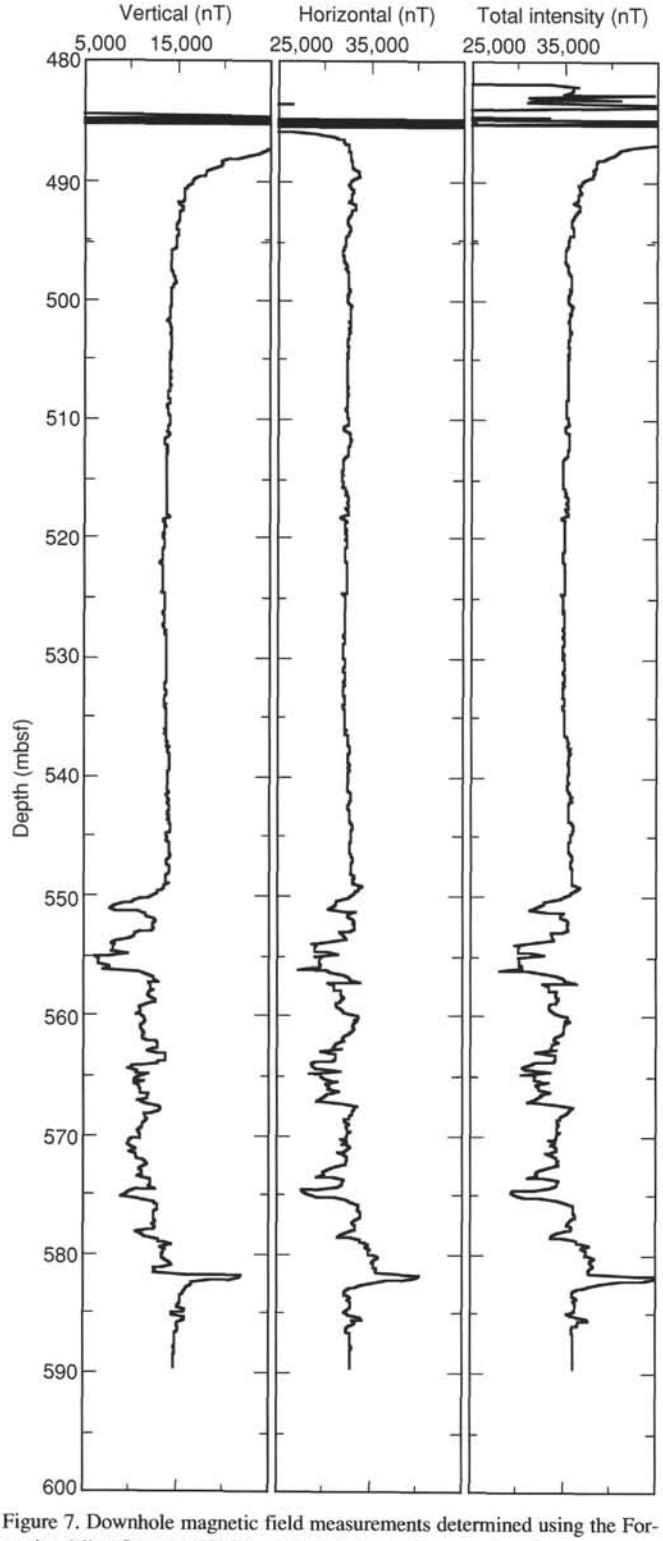

Figure 7. Downhole magnetic field measurements determined using the Formation MicroScanner (FMS), three-axis fluxgate magnetometer instrument. The three-component magnetic data (FX is the horizontal "*x*" component, parallel to the FMS Pad 1 direction; FY is the horizontal "*y*" component, perpendicular to the Pad 1 direction; and FZ is the vertical "*z*" component) enable one to calculate horizontal and vertical intensities, inclination, and relative declination. From about 550 to 580 mbsf, sharp decreases are seen in both the vertical and horizontal components of the downhole magnetic field. Below about 580 mbsf, sharp increases in both the vertical and horizontal components of the downhole magnetic field appear.

Wallick, 1992; Wallick and Steiner, 1992). The sharp, well-correlated increases in both the vertical and horizontal components below about 580 mbsf imply normal-polarity magnetization obtained in the same manner and are consistent with the core samples recovered in that interval.

Detailed post-cruise analyses, including model calculations based on the disk model (Hamano and Kinoshita, 1990), will be necessary to explain both the short wavelength variation and the amplitude ratio of horizontal intensity component to vertical intensity component.

Temperature Measurements

At Hole 801C, we ran a Lamont-Doherty temperature tool (see "Explanatory Notes" chapter, this volume) on the bottom of the first logging string and recorded ambient pressure and temperature along with elapsed time as the tool descended into the hole and returned to the surface. This should be a good measure of thermal equilibrium in the water column of the borehole, because it has not been disturbed in the 2.5 yr since it was drilled. To disturb the ambient water temperature only a minimal amount, the drill string was lowered about 100 m into the casing before this logging run. During its descent, we stopped the drill string for a period of 5 min at the seafloor (5685 mbrf) so that we would obtain a clear plateau in our pressure-vs.-time record. We stopped it again at 6100 mbrf to engage the heave compensator and pulled it up slightly to test the compensator. At 6281 mbrf, the drill string reached the bottom of the hole and upward logging began. Using two methods (one with the length of wire out and the pressure recorded with the tool at the seafloor, and the second with the length of wire out and the pressure recorded with the tool on the bottom), we interpolated depths for the tool at all intermediate pressures. From this interpolation, we were able to draw a curve for temperature vs. depth (Fig. 8).

This temperature-vs.-depth curve shows a gradient of approximately 30°/km in the lower 250 m of the hole. The upper part of the hole in the casing shows a somewhat steeper thermal gradient of approximately 46°/km. These gradients suggest that at this time no net flow of water is seeping down the hole into Jurassic basement.

Permeability Measurements

Hydrogeologic characteristics were studied at Hole 801C using a drill-string packer manufactured by TAM, International. This nonrotatable, straddle packer was used in the single-element mode to determine permeability within the Jurassic oceanic basement at Hole 801C. The packer is inflated against the borehole wall to isolate the portion of the borehole below the pack-off point, and controlled pressure is applied to this lower part of the hole by pumping water down the drill pipe. When pumping ceases, the rate at which the excess pressure decays is related to the permeability of the formation being tested.

Two downhole pressure gauges and clocks were tested and calibrated, and the draw-works plumbing was pressure-tested before downhole operations. Our strategy was to determine permeability below two levels in Hole 801C. First, we would test almost the entire length of the hole by seating the packer just below the bottom of the casing, and then again the portion of the hole beneath the hydrothermal unit that separates the upper alkali basalts from the lower tholeiitic basalts about halfway down the hole. Thus, initially, the packer element was placed at 501 mbsf, 20 m below the bottom of casing at 481 mbsf. All depths refer to those established during Leg 129, assuming a seafloor depth of 5685 mbrf and a depth to the bottom of casing of 6166 mbrf.

Downhole operations started at 0212Z, 25 June 1992 (all subsequent times are in GMT or Z, 25 June 1992) when we installed and time-zeroed Kuster Clock #K4051 in a 15,200-psi

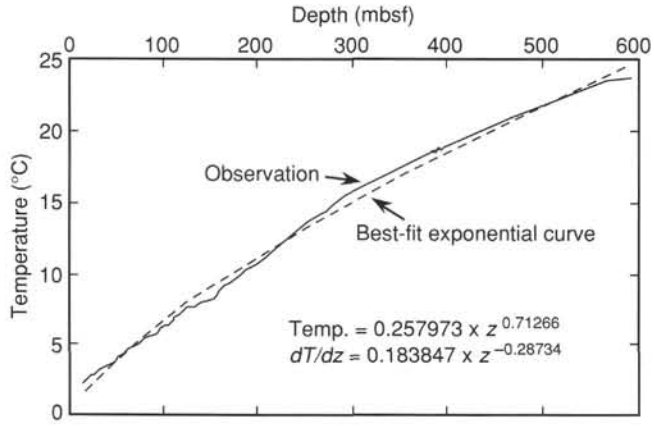

Figure 8. Plot of undisturbed bottom-water temperature vs. depth in Hole 801C, measured 2.5 yr after the hole was drilled. The data show a relatively continuous, upward-increasing temperature gradient within the open hole below 481 mbsf, and up into casing at least to 230 mbsf. The temperature gradient is relatively constant above 230 mbsf.

Kuster downhole pressure gauge. The go-devil containing these tools was dropped at 0226Z and landed at the BHA at 0300Z (Fig. 9). The increase in pressure to 100–150 psi from seating the go-devil was monitored from 0300Z to 0318Z and found to be steady, indicating a good seat. At 0318Z, the packer element was inflated to 1500 psi, which also held steady, indicating a good inflation and packer seat. At 0329Z, 15,000 lb of drill collar weight was shifted onto the packer element, which allowed the excess pressure to flow downhole below the packer into the portion of the borehole to be tested. The uphole pressure was observed to decrease almost immediately to <50 psi, indicating a highly permeable formation somewhere below the packer seat, or that the packer seat was leaking. Uphole pressure decayed rapidly to about 10 psi, and at 0334Z and 0336Z, two pulse tests were conducted. Pressure was increased suddenly to 800 and 1800 psi, respectively, and was seen to decay very rapidly in both cases, also indicating high permeability in the formation. Throughout this interval, the packer continued to support a steady 15,000 lb of drill collar load, and the drill string remained immobile, indicating a good mechanical connection of the packer element to the borehole wall. This implied that the packer seat was sealed as well, indicating that the apparent high permeability was within the Jurassic basement below the packer.

Thus, we assumed high permeability and decided to investigate further with injection testing by continuous pumping. We first pumped a total of 741 strokes at 50 spm (strokes per minute) from 0339Z to 0354Z (one stroke = 5 gal = 18.9 L) and then ceased pumping. Uphole pressure decayed immediately from 600 to <100 psi, and then decayed more slowly to 10 psi by 0405Z.

This low pressure was monitored until 0427Z when we began the second injection test. At 0427Z we began pumping at 75 strokes/min and continued to pump until 0451Z. During this 24-min period we pumped a total of 1755 strokes (33,170 L) into the hole, achieving a final pressure of 1200 psi. When pumping ceased at 0451Z, the uphole pressure dropped immediately to about 200 psi, and then decayed more slowly to 10 psi by 0525Z. Packer deflation was initiated at 0530Z.

To check that the apparently high permeability was not from a leaking packer seal, the packer was deflated, the drill string was lifted 2 m, and the packer was reset at 499 mbsf (Fig. 10). At 0555Z, the packer was reinflated to 1500 psi, and this pressure held constant until 0604Z. The packer then was set with a 15,000 lb. load of drill collars. As before, pressure decayed to <50 psi immediately, whereas the packer held the 15,000 lb load and the drill string remained immobile. At 0611Z, 0623Z, and 0638Z, pulse tests were conducted by sudden pressure loads of 1000 to 1500 psi. In each case, the pressure dropped immediately to <50 psi when pumping ceased and to 10 psi within the next 5 min. We concluded that the formation below the packer contained an extremely permeable zone and began to deflate the packer at 0654Z.

The go-devil was retrieved, and we discovered that no useful downhole pressure data had been recorded by the Kuster tools, apparently because Clock #K4051 was operating abnormally rapidly. The intended 6-hr record was traversed in about 1 hr, soon after the clock was installed. We then decided to run a backup pressure gauge rated at 12,050 psi along with the 15,200 psi gauge during the next run. Hydrostatic pressure at the bottom of the hole was about 9400 psi; thus, the lower pressure instrument would have been near its load limit during the setting of the packer. Clock #K4051 was installed with the 12,050 psi gauge, and Clock #K4080 was installed with the 15,200 psi gauge at 0948Z.

The packer was lowered to 542 mbsf, within the upper portion of the tholeiitic basalt sequence and below the hydrothermal deposit. The hydrothermal unit indicated by our logs seemed to be somewhat thicker than that determined by core recovery during

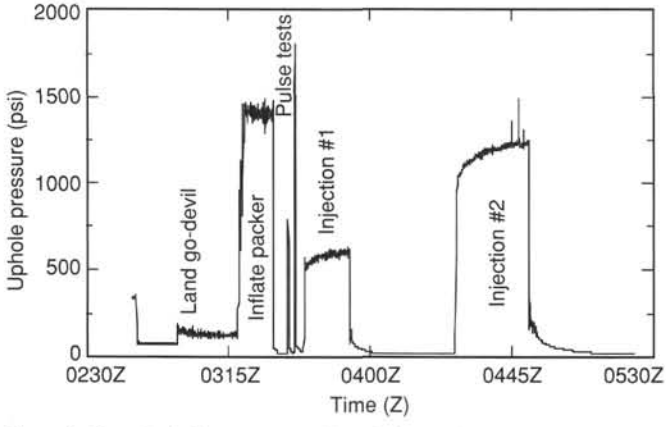

Figure 9. Plot of uphole pressure vs. time during packer measurements, with the packer set at 501 mbsf. The operations recorded include (in time sequence order) the go-devil landing, packer inflation, two pulse tests, and two constant-flow injection tests.

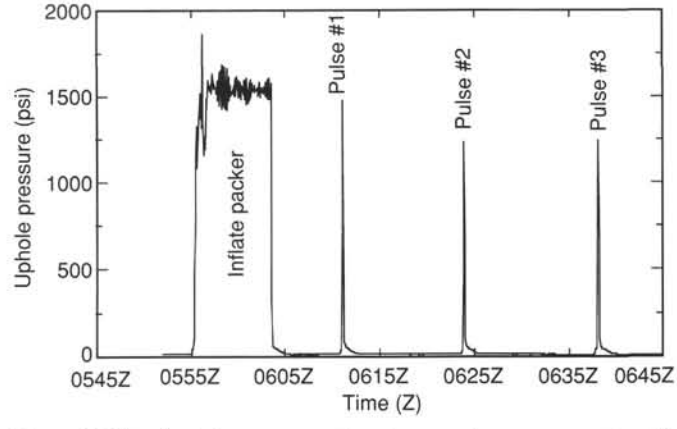

Figure 10. Plot of uphole pressure vs. time during packer measurements, with the packer set at 499 mbsf. The operations recorded include (in time sequence order) packer inflation and three pulse tests.

Leg 129, as it extended from at least 514 to 530 mbsf, and we suspected that this was the main zone of high permeability below the upper packer seats.

A go-devil containing two downhole pressure gauges was dropped down the drill string at 1013Z and landed at the BHA at 1047Z, as evidenced by a constant pressure increase to 150–200 psi from 1047Z to 1058Z. Packer inflation was the attempted, but the drill string responded by moving 3.5 m uphole when pressure was raised to 1200 psi. The packer element was allowed to deflate until 1123Z, when inflation was again attempted with the same result. In addition, the packer element would not hold pressure when pumping stopped, indicating either that the packer seal was leaking or that the packer element had ruptured. A third inflation was attempted at 1153Z with the same results. To check that the packer element had really ruptured, we attempted to reset it at 500 mbsf, where we had been successful originally. There, the system would not hold pressure when pumping ceased, but the drill string did not ride uphole, indicating that we were dumping the excess pressure through the ruptured packer element and into the permeable hydrothermal zone that was now below the BHA.

When the BHA was retrieved, we discovered that the packer element had indeed ruptured, that Kuster Clock #K4051 had run fast a second time, and that Kuster Clock #K4080 provided an accurate downhole pressure record of our attempts to seat a ruptured packer element.

We tentatively conclude that Hole 801C is highly permeable somewhere below 501 mbsf. The zone of high permeability is probably associated with the highly porous portions of the hydrothermal zone at 510–520 and 525–530 mbsf. The portion of the hole below 542 mbsf is relatively impermeable, but this conclusion is based on observations of drill-pipe behavior during pressure testing and cannot be quantified. Although downhole pressures were not recorded, quantitative studies of the uphole pressure and pumping records can be used in conjunction with other studies of high-permeability zones to quantify the high-permeability region. These studies will demonstrate that, contrary to prior assumptions, old oceanic crust can be highly permeable, although these permeable layers may be restricted to fossilized hydrothermal systems.

REFERENCES *

Anderson, R.N., Langseth, M.G., and Sclater, J.G., 1977. The mechanisms of heat transfer through the floor of the Indian Ocean. *J. Geophys. Res.*, 82:3391–3409.

Becker, K., Langseth, M.G., Von Herzen, R.P., Anderson, R.N., and Hobart, M.A., 1985. Deep crustal geothermal measurements, Hole 504B, Deep Sea Drilling Project Legs 69, 70, 83, and 92. *In* Anderson, R.N., Honnorez, J., Becker, K., et al., *Init. Repts. DSDP*, 83: Washington (U.S. Govt. Printing Office), 405–418.

Carlson, R.L., and Herrick, C.N., 1990. Densities and porosities in the oceanic crust and their variations with depth and age. *J. Geophys. Res.*, 95:9153–9170.

COSOD II, 1987. *Report of the Second Conference on Scientific Ocean Drilling, Strasbourg, France* (European Science Foundation, JOIDES and JOI).

Fehn, U., 1986. The evolution of the low-temperature convection cells near spreading centers: a mechanism for the formation of Galapagos Mounds and similar manganese deposits. *Econ. Geol.*, 81:1396–1407.

Fehn, U., and Cathles, L., 1986. The influence of plate movement on the evolution hydrothermal convection cells in the oceanic crust. *Tectonophysics*, 125:289–312.

Fisher, A.T., Becker, K., Narasimhan, T.N., Langseth, M.G., and Mottl, M.J., 1990. Passive, off-axis convection through the southern flank of the Costa Rica rift. *J. Geophys. Res.*, 95:9343–9370.

Floyd, P.A., and Castillo, P.R., 1992. Geochemistry and petrogenesis of Jurassic ocean crust basalts, Site 801. *In* Larson, R., Lancelot, Y., et al., *Proc. ODP, Sci. Results*, 129: College Station, TX (Ocean Drilling Program), 361–388.

Gallet, Y., and Courtillot, V., 1989. Modeling magnetostratigraphy in a borehole. *Geophysics*, 54:973–983.

Hamano, Y., and Kinoshita, H., 1990. Magnetization of the oceanic crust inferred from magnetic logging in Hole 395A. *In* Detrick, R., Honnorez, J., Bryan, W.B., Juteau, T., et al., *Proc. ODP, Sci. Results*, 106/109: College Station, TX (Ocean Drilling Program), 223–229.

Larson, R.L., Pitman, W.C., Golovchenko, X., Cande, S.C., Dewey, J.F., Haxby, W.F., and LaBrecque, J.L., 1985. *The Bedrock Geology of the World:* New York (Freeman).

Larson, R.L., and Sager, W.W., 1992. Skewness of magnetic anomalies M0 to M29 in the northwestern Pacific. *In* Larson, R.L., Lancelot, Y., et al., *Proc. ODP, Sci. Results*, 129: College Station, TX (Ocean Drilling Program), 471–481.

Morton, J.L., and Sleep, N.H., 1985. A mid-ocean ridge thermal model: constraints on the volume of axial hydrothermal heat flux. *J. Geophys. Res.*, 90:11345–11353.

Mottl, M.J., Lawrence, J.R., and Keigwin, L.D., 1983. Elemental and stable-isotope composition of pore waters and carbonate sediments from Deep Sea Drilling Project Sites 501/504 and 505. *In* Cann, J.R., Langseth, M.G., Honnorez, J., Von Herzen, R.P., White, S.M., et al., *Init. Repts. DSDP*, 69: Washington (U.S. Govt. Printing Office), 461–473.

Pringle, M.S., 1992. Radiometric ages of basaltic basement recovered at Sites 800, 801, and 802, Leg 129, western Pacific Ocean. *In* Larson, R.L., Lancelot, Y., et al., *Proc. ODP, Sci. Results*, 129: College Station, TX (Ocean Drilling Program), 389–404.

Shipboard Scientific Party, 1990. Site 801. *In* Lancelot, Y., Larson, R., et al., *Proc. ODP, Init. Repts.*, 129: College Station, TX (Ocean Drilling Program), 91–170.

Steiner, M.B., and Wallick, B.P., 1992. Jurassic to Paleocene paleolatitudes of the Pacific plate derived from the paleomagnetism of the sedimentary sequences at Sites 800, 801 and 802. *In* Larson, R.L., Lancelot, Y., et al., *Proc. ODP, Sci. Results*, 129: College Station, TX (Ocean Drilling Program), 431–446.

Wallick, B., and Steiner, M.B., 1992. Paleomagnetic and rock magnetic properties of Jurassic Quiet Zone basalts, Hole 801C. *In* Larson, R.L., Lancelot, Y., et al., *Proc. ODP, Sci. Results*, 129: College Station, TX (Ocean Drilling Program), 455–470.

Williams, D.L., Von Herzen, R.P., Sclater, J.G., and Anderson, R.N., 1974. The Galapagos spreading centre: lithospheric cooling and hydrothermal circulation. *Geophys. J. R. Astron. Soc.*, 38:587–608.

* Abbreviations for names of organizations and publication titles in ODP reference lists follow the style given in *Chemical Abstracts Service Source Index* (published by American Chemical Society).

144IR-110

NOTE: Conventional log, FMS, dipmeter, and geochemical log (element and oxide weight %) data can be found in CD-ROM form (back pocket).

Hole 801C: Resistivity-Velocity-Natural Gamma Ray Log Summary

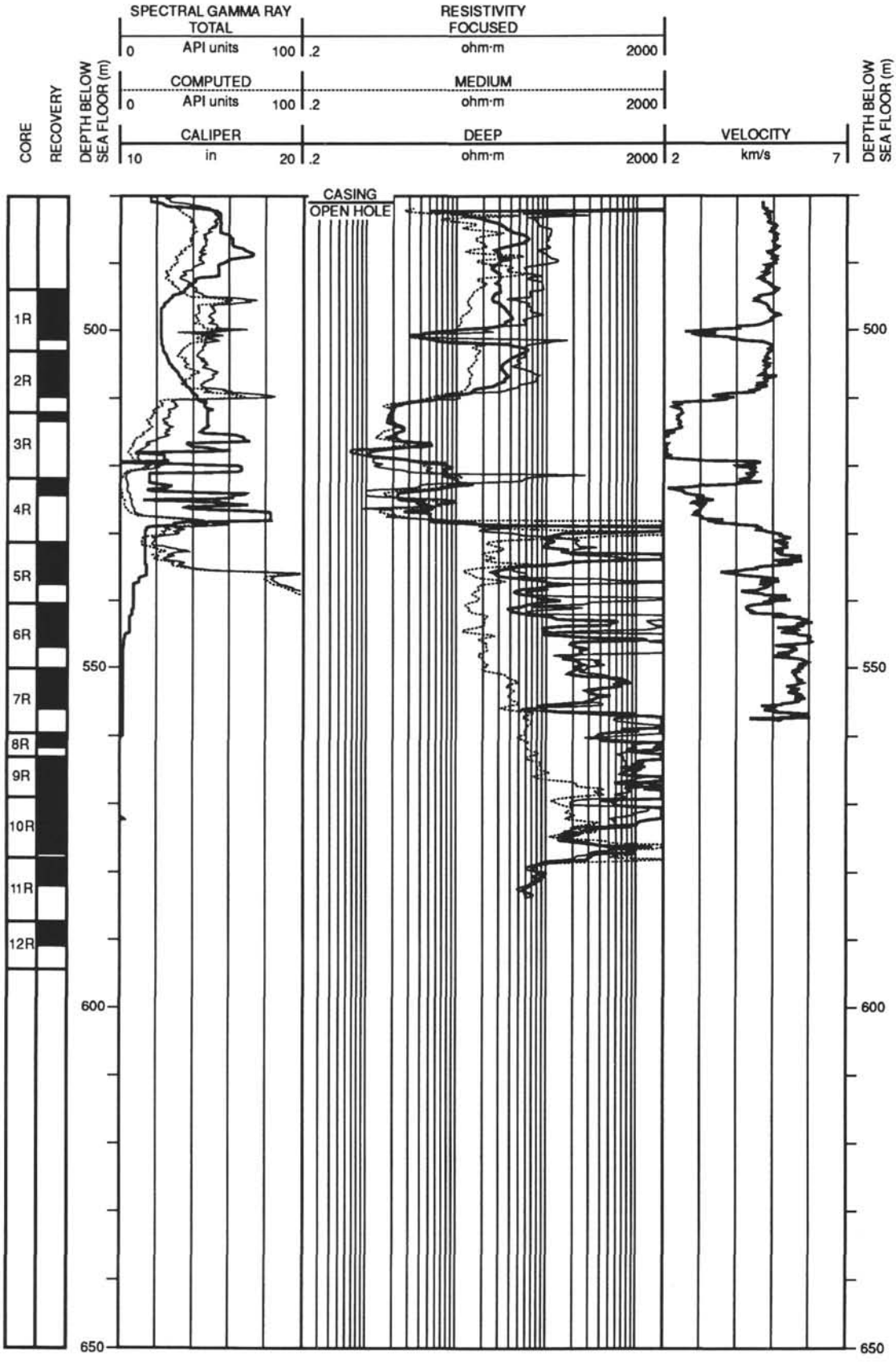

Hole 801C: Density-Porosity-Natural Gamma Ray Log Summary

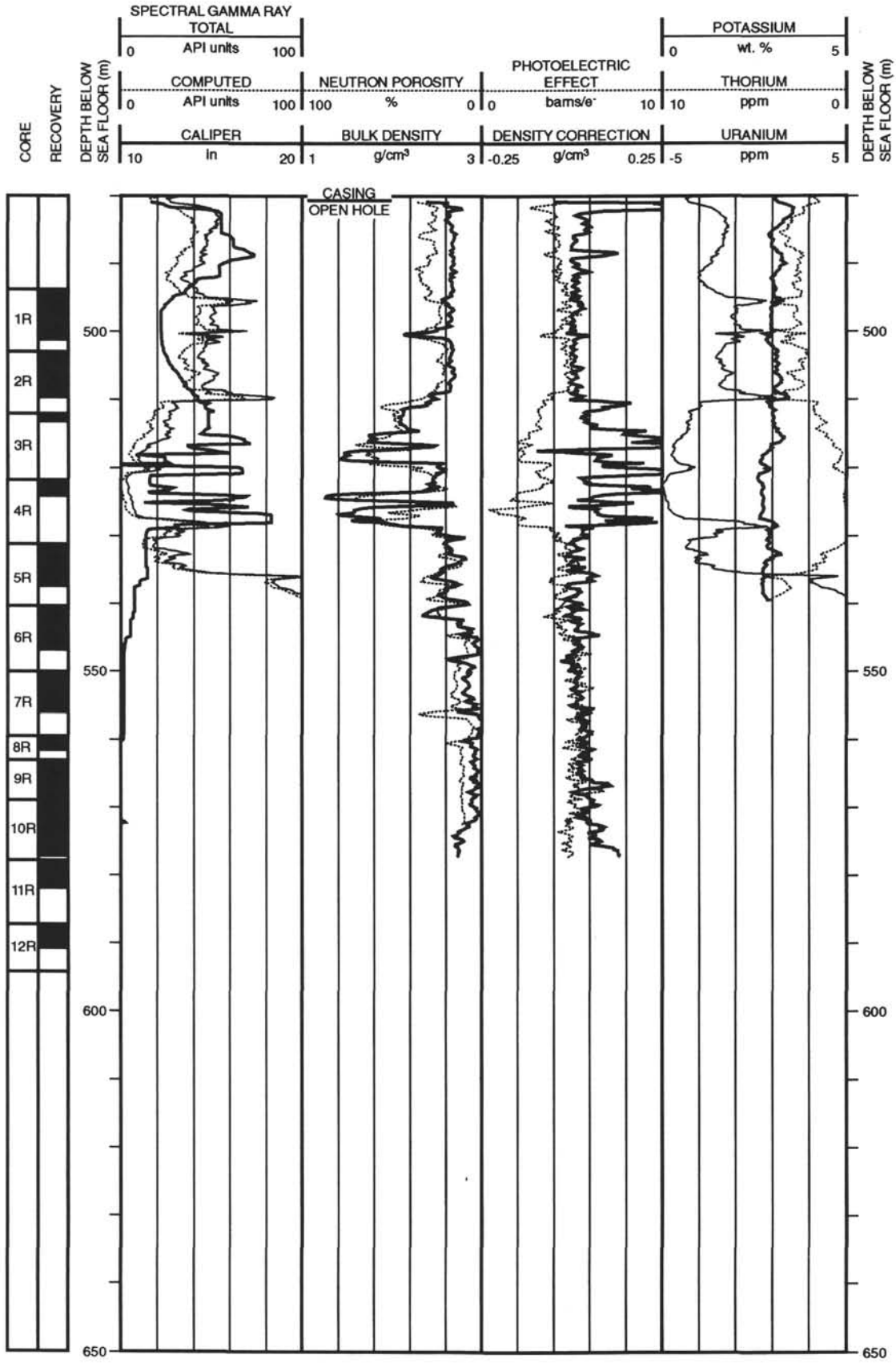

Hole 801C: Geochemical Log Summary

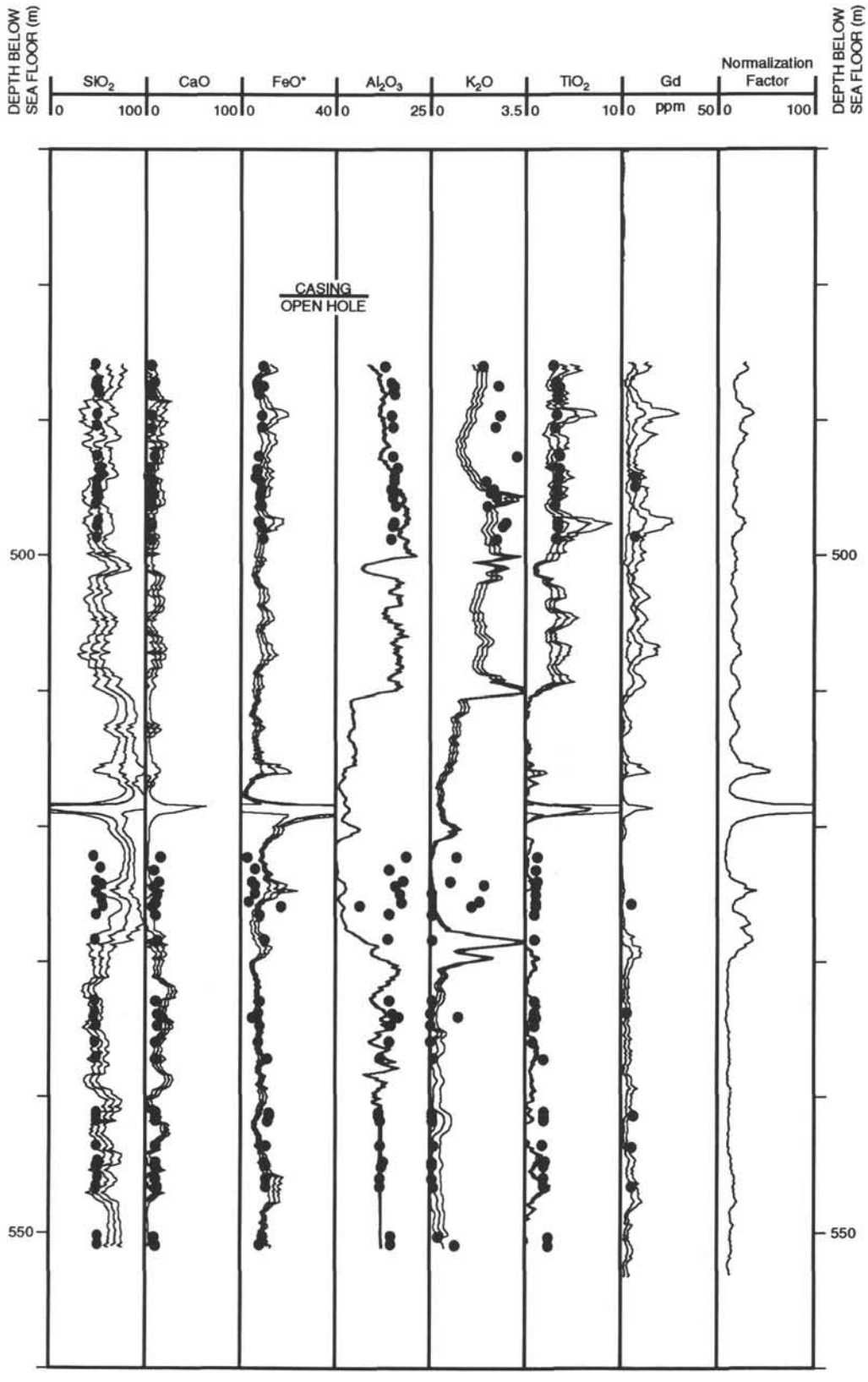

Hole 801C: Geochemical Log Summary